A Silent Microwave Drill for Deep Holes in Concrete

Eli Jerby, Yuri Nerovny, Yehuda Meir, Or Korin, Ron Peleg, and Yariv Shamir

***Abstract*— This paper presents a mechanically assisted microwave drill (MWD) capable of drilling 26-cm-deep 12-mm-diameter holes in concrete. This record significantly extends the inherent λ/4-depth capability (∼1.5 cm at 2.45 GHz) of the basic MWD scheme. Compared with conventional mechanical drills, this MWD is characterized by a relatively silent and vibration-free operation, but its drilling speed is yet slower than 1 cm/min. This paper reviews the fundamental MWD mechanism (utilizing localized microwave heating and thermal-runaway instability), and extends it for deeper holes by also using the coaxial applicator as a slowly rotating hollow reamer to remove the debris. The MWD prototype is introduced, including its adaptive impedance matching and remote-operation features, and its experimental results are presented. Theoretical and practical MWD aspects are discussed, and potential developments are indicated (e.g., for faster drilling and iron-rebar cutting). The present MWD performance can be useful for specific applications which critically require silent drilling operations in concrete.**

***Index Terms*— Autotuner, concrete, construction tools, hotspot, localized microwave heating, microwave drill (MWD), thermal drilling.**

I. Introduction

CONSTRUCTION, as well as industrial and geological operations, often requires drilling holes in solids. Mechanical drill-bits are widely used for these purposes, but their fast rotation typically produces noise, vibrations, and dust effusion. Other drilling technologies, using lasers, water jets, electrical discharges, chemicals, ultrasonic vibrations, plasma streams, etc., are yet more expensive or less adequate for field applications such as concrete drilling [1]–[6].

Microwave implementations for material processing have been studied and developed for a wide range of industrial, scientific, and medical applications [7], [8]. In particular, microwave applications have been developed for cement and concrete processing [9]–[11], including microwave-assisted curing processes [12], recycling of concrete demolition waste [13], concrete heating processes [14], and microwave furnaces for cement manufacturing [8].

One of the difficulties involved in volumetric microwave heating is the accidental effect of thermal-runaway instability [15], [16]. This nonuniform heating effect may cause a local rapid increase of the temperature, and hence a hotspot which may damage the processed material.

The microwave drill (MWD) concept [17]–[19] intentionally utilizes the thermal-runaway instability in order to concentrate the microwave-heating energy into a hotspot, much smaller than the microwave wavelength, λ. As illustrated in Fig. 1(a), the hotspot region is rapidly softened or even melted, and the center electrode is mechanically inserted into it, in order to make the hole [20]. The basic MWD mechanism does not require fast rotating parts, and it makes no dust or noise. Its effective drilling depth is limited, however, to $\sim\lambda/4$ ($\sim$1.5 cm at 2.45 GHz in concrete) since the broadside radiation pattern in deeper penetration depths impedes its further progress [20].

MWD's have been studied in a variety of materials, such as glass, ceramics, and bones [21]. A solid-state MWD [22] has demonstrated a microwave-drilling feasibility at ∼0.1-kW power, for e.g., ∼1-mm-diameter ∼4-mm-deep holes in glass. In a wider scope, the MWD approach is extended by the localized microwave-heating (LMH) paradigm [23] to other applications, such as cutting, joining, additive manufacturing, combustion, plasma, and nanopowder generation [24].

Here we present the MWD extension beyond the $\lambda/4$ depth, demonstrated by a silent, remotely operated MWD prototype for concrete and masonry. Various aspects of this work have been introduced in conferences [25], [26], and here we present

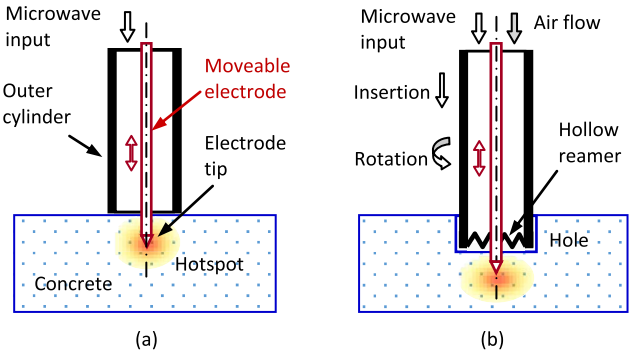

Fig. 1. Conceptual schemes of MWD applicators. (a) Basic MWD consists of a coaxial waveguide with a moveable center electrode, inserted into the softened hotspot to form the hole. (b) Advanced MWD for deeper holes. The hotspot is further extended in order to enable the removal of the softened debris by the slowly rotating outer cylinder as a hollow reamer, assisted by inner pressurized-air flow.

Manuscript received March 27, 2017; revised June 10, 2017; accepted July 5, 2017. Date of publication August 7, 2017; date of current version January 4, 2018. This work was supported by the Israel Science Foundation under Grant 1270/04, Grant 1639/11, and Grant 1896/16. *(Corresponding author: Eli Jerby.)*

The authors are with the Faculty of Engineering, Tel Aviv University, Ramat Aviv 6997801, Israel (e-mail: jerby@eng.tau.ac.il).

This paper has supplementary downloadable material available at http://ieeexplore.ieee.org, provided by the authors. The supplementary file includes a video. The video clip shows the initial stage of the microwave-drill operation in concrete. The hotspot is created by the localized microwave-heating (LMH) effect, hence the concrete is locally melted there. The outer conductor of the coaxial waveguide (12-mm diameter) functions also as a hollow reamer. It is slowly rotating in order to silently remove the softened concrete and to deepen the hole. This mechanically-assisted microwave-drill bit penetrates further into the concrete hence the hotspot progressing deeper inside is no longer seen on the surface. This combined microwave-mechanical mechanism enables silent drilling of >20-cm deep holes in concrete. The file size is 1.04 MB.

Color versions of one or more of the figures in this paper are available online at http://ieeexplore.ieee.org.

Digital Object Identifier 10.1109/TMTT.2017.2729509

a comprehensive report on this paper, including a theoretical aspect and additional experiments. In the following sections, the MWD principle is reviewed and its implementation is extended to deeper holes. An experimental, remotely controlled MWD prototype is described, and considerations for its further development are discussed.

II. Extended Microwave-Drill Principles

The basic MWD scheme [17] exploits the thermal-runaway instability in order to drill shallow holes in nonmetallic substrates. The microwave energy is directed to the drilled region by a coaxial waveguide with a movable center electrode, as illustrated in Fig. 1(a). The LMH effect is attributed to the temperature dependence of the material properties [e.g., the dielectric permittivity, $\varepsilon(T)$] [20], [27]. Due to the thermal runaway, the energy absorption rate is faster than the cooling caused by the thermal conductivity; hence a well-confined hotspot is rapidly evolved underneath the electrode tip in the solid material. The center electrode is mechanically inserted then into the softened hotspot region, to form the hole.

The basic MWD concept is extended here in order to enable drilling holes much deeper than $\lambda/4$. For this purpose, the outer coaxial cylinder also functions as a slowly rotating hollow reamer, hence enabling the insertion of the entire coaxial applicator into the drilled substrate. In this mechanically assisted MWD operation, illustrated in Fig. 1(b), the electrode tip is kept sufficiently close to the outer cylinder face, hence its optimal $\sim\lambda/4$ protrusion is also maintained in deeper holes. The debris are mechanically removed during the MWD operation in order to enable the entire drilling-tube insertion, hence to further deepen the hole.

A theoretical model is applied here in order to evaluate the feasibility of LMH process in concrete. The model couples the electromagnetic (EM) wave equation and the heat equation in the region in front of the drill-bit aperture. This model [20] is valid for the initial period of the hotspot formation, before melting, in the basic scheme depicted in Fig. 1(a). The two time-scale approximation [20] allows the solution of the EM-wave equation in the frequency domain and the heat equation in the time domain. (Since the temperature variation is much slower than the EM wave.) Hence, the nonlinear-coupled set of equations is simplified to the form

$$\nabla \times \nabla \times \tilde{\mathbf{E}} - (\varepsilon_r' - j\varepsilon_r'')k_0^2\tilde{\mathbf{E}} = 0 \tag{1}$$

$$\rho c_p \partial T/\partial t - \nabla \cdot (k\nabla T) = \pi f \varepsilon_0 \varepsilon_r'' |\tilde{\mathbf{E}}|^2 \tag{2}$$

where $\tilde{\mathbf{E}}$, k_0, and f are the electric-field vector, wavenumber, and frequency, respectively, of the EM wave. The drilled material is characterized by $\varepsilon(T) = \varepsilon_0(\varepsilon_r' - j\varepsilon_r'')$, ρ, c_p, and k, namely, the dielectric permittivity, density, heat capacity, and thermal conductivity, respectively. Equations (1) and (2) are coupled by both $\tilde{\mathbf{E}}$ and $\varepsilon(T)$, and they are solved by finite differences in order to simulate the temporal and spatial evolution of the hotspot temperature profile.

The temperature-dependent dielectric permittivity of concrete [28] is approximated by

$$\varepsilon(T) = \varepsilon_0 \sum_{n=0}^{N} (a_n - jb_n)(T - T_{\mathrm{RT}})^n \tag{3}$$

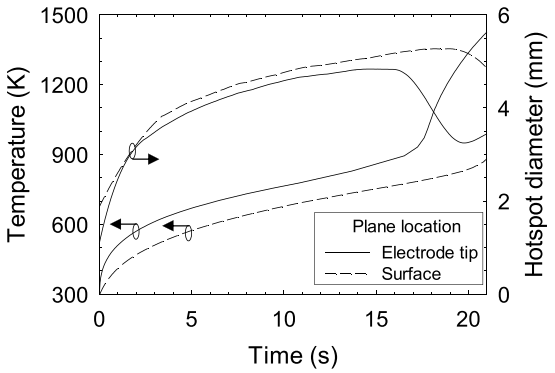

Fig. 2. Simulated hotspot evolution in concrete. The peak temperature attained and the hotspot size (FWHM) are presented in two planes perpendicular to the electrode axis; one at the electrode-tip level (4 mm deep), and the other on the entrance surface (in solid and dashed curves, respectively). The thermal-runaway effect is noticed at $t \sim 18$ s.

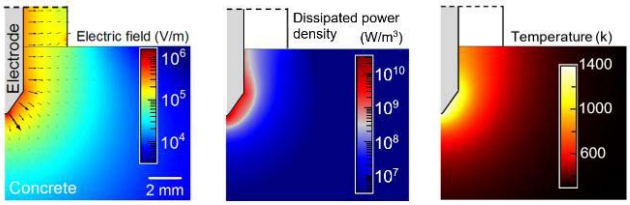

Fig. 3. Simulated profiles of (a) hotspot's electric-field localization, (b) dissipated power density, and (c) localized temperature at $t = 20$ s in the conditions of Fig. 2 above.

where the best-fit polynomial coefficients for $N = 5$ are $a_{0-5} = 4.33;\ -6.9 \cdot 10^{-3};\ 2 \cdot 10^{-5};\ -3 \cdot 10^{-8};\ 10^{-11};\ 4 \cdot 10^{-15}$, $b_{0-5} = 0.1;\ -0.7 \cdot 10^{-3};\ 4 \cdot 10^{-6};\ -9 \cdot 10^{-9};\ 9 \cdot 10^{-12};\ -2 \cdot 10^{-15}$, and $T_{\mathrm{RT}} = 300$ K. The other parameters are assumed constant, $k = 1.4$ W/m K, $c_p = 880$ J/kg K, and $\rho = 2,210$ kg/m^3 [29]. The simulated microwave frequency and incident power are $f = 2.45$ GHz and $P_{\mathrm{Inc}} = 0.85$ kW, respectively.

The simulated hotspot evolution is presented in Fig. 2 by the peak temperature increase, and the corresponding size [full-width half-maximum (FWHM)] of the heat-affected zone (HAZ). The electrode diameter and the cylinder inner diameter are 2 and 8 mm, respectively. The center electrode is inserted 4 mm into the concrete (in a fixed position). For the sake of comparison, the variables are shown in two different planes perpendicular to the electrode axis; at the electrode-tip level and on the entrance surface (namely, at 4- and 0-mm depths, respectively). The knee at $t \sim 18$ s in the graph, where the heating rate near the electrode tip is abruptly increased (and the hotspot begins to shrink), indicates a thermal-runaway instability. On the entrance surface, the hotspot appearance is deemed by the thermal conductivity and air cooling.

The hotspot localization is shown in Fig. 3(a)–(c), simulated in the conditions of Fig. 2 at $t = 20$ s. The resulted electric-field distribution, dissipated power density, and temperature profile, are presented along the hotspot's axial cross section. The electric field [Fig. 3(a)] attains a maximal value of $\sim$6 kV/cm. The absorbed microwave power [Fig. 3(b)] results in $\sim$50-W total, due to the impedance mismatch and power reflections. The temperature profile [Fig. 3(c)] confirms the

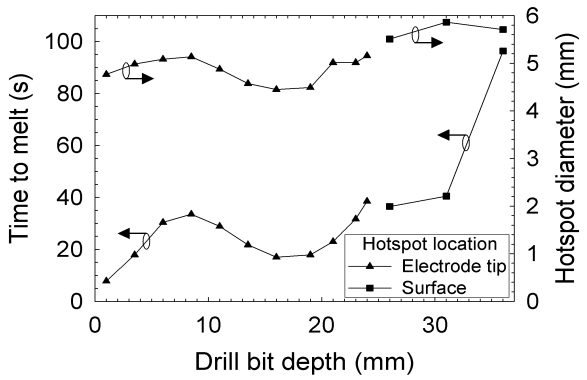

Fig. 4. TTM and the hotspot FWHM size as a function of the electrode-tip depth in the concrete (in static conditions). In a deeper penetration of the center electrode (>25-mm protrusion), the hotspot is evolved on the outer surface rather than around the electrode tip.

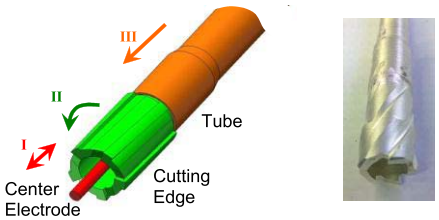

(a) (b)

Fig. 5. MWD tube used for deep holes in concrete, as a hybrid of a coaxial open-end microwave applicator and a hollow reamer. (a) Center electrode is inserted into the hotspot evolved in front of it (I), and further softens the concrete. The debris is removed by the slowly rotating hollow reamer (II), which enables the axial progress of the entire drilling tube (III). (b) Silver-coated 12-mm diameter grooved outer cylinder.

hotspot evolution in front of the electrode tip, exceeding the concrete's melting point.

The effect of the drill-bit depth on the hotspot evolution is simulated in Fig. 4. The time-to-melt (TTM) period and the consequent HAZ size are calculated at various depths of the drill bit inside the concrete. The results confirm that the optimal drill-bit depth in these conditions, where both the TTM and HAZ size attain their minimal values, is ~16 mm (nearly $\lambda/4$ in concrete). In depths over 25 mm, the hotspot is no longer evolved in front of the drill bit, but rather near the entrance surface. The HAZ size is wider there, and the localization effect is slower and weaker, hence the basic MWD [Fig. 1(a)] is no longer effective in >25-mm depths.

The numerical analysis also shows the critical need for an adaptive impedance matching, due to the rapid changes in the load condition during its operation. The mismatched input impedance may vary within seconds from relatively high-to-low impedance, in the transition from cold to molten substrate (or open to short circuit), respectively. Hence, an adaptive impedance autotuning [30] is essential in order to minimize the power reflections and to optimize the MWD effectiveness

III. Experimental Setup

The mechanically-assisted MWD scheme, illustrated in Fig. 1(b), is implemented by the drill-bit shown in Fig. 5(b). This silver-coated hard-metal tube (12-mm outer diameter, 30 cm long) is corrugated with helical grooves on its outside.

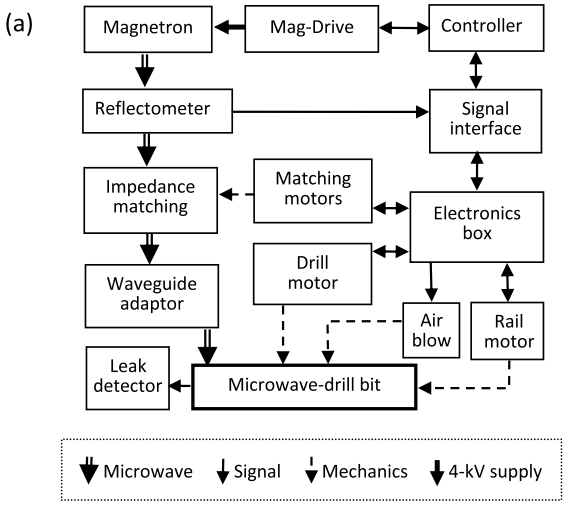

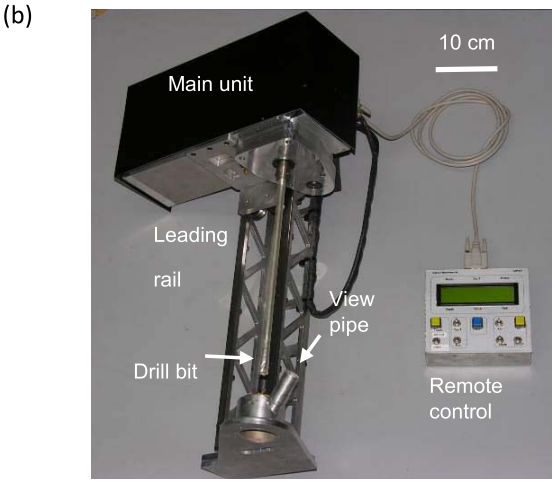

Fig. 6. Overview of the MWD portable prototype (a) Block diagram of the main microwave, electronics, and mechanical functions. (b) Experimental MWD prototype.

With a movable center electrode inside, this coaxial structure transfers the microwave power to the drilled region in order to form the hotspot. In addition, it slowly rotates (at <20 r\min) hence it also functions as a hollow reamer removing the debris. As an option, pressurized air is blown through the coaxial structure in order to assist the debris removal and to cool down the tube.

The synchronized MWD operation includes the center electrode insertion [marked I in Fig. 5(a)] into the softened hotspot in order to maintain its optimal ~$\lambda/4$ lead (~1.5 cm). The slow rotation of the outer cylinder [marked II in Fig. 5(a)] simultaneously cuts the softened concrete in the hotspot margin, and further deepens the hole. The axial motion marked III in Fig. 5(a) inserts the entire coaxial structure into the extended hole. This motion is conditioned by the sufficient softening of the concrete in this region (as described in the following).

The block diagram depicted in Fig. 6(a) presents the main components of the MWD prototype, including its microwave, electronics and mechanical functions (developed by Scilense Microwave Ltd., Israel). The overview image in Fig. 6(b) shows the drilling tube, the leading rail, the main unit, and the operating box. The drilling tube [Fig. 5(a) and (b)]

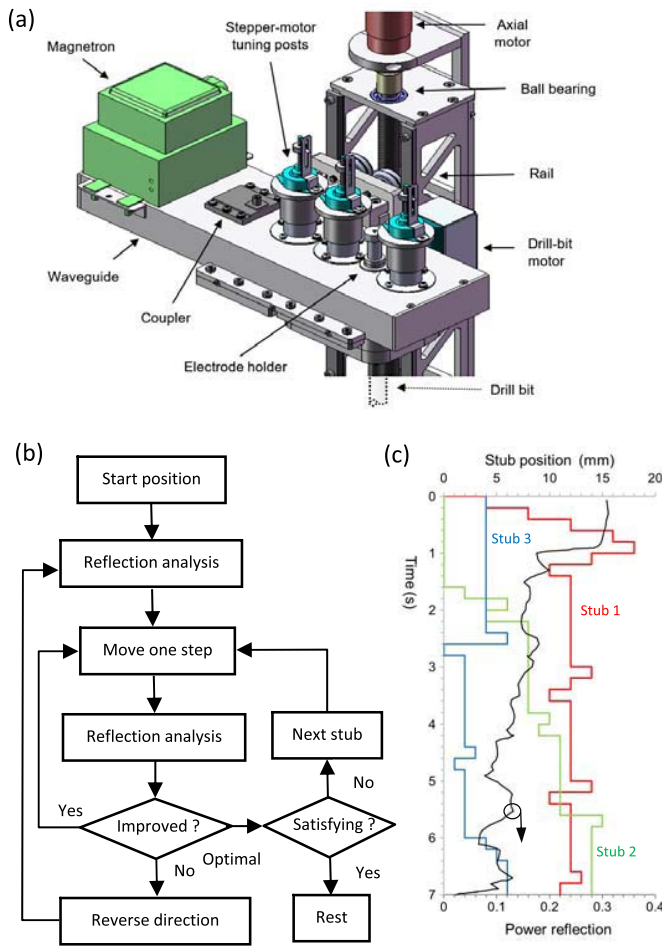

Fig. 7. Adaptive impedance-matching tuning. (a) Triple-stub section with the waveguide-to-coax transition between the second and third stubs. (b) Tuning algorithm executed by the programmable controller driving the stubs' stepper motors. (c) Typical sequence of the three-stub position variation (in ∼0.2-s step period) and the consequent reduction of the reflection coefficient.

is installed by a chuck on the main unit. The 0.85-kW 2.45-GHz magnetron is fed by a controllable switched-mode power supply (MagDrive 1000, Dipolar, Sweden).

The adaptive impedance matching and the other MWD functions are automatically executed by a programmable controller embedded in the MWD system. For instance, the axial insertion motion [marked III in Fig. 5(a)] is dictated by a feedback loop that measures the torque applied in the rotation motion [marked II in Fig. 5(a)]. This loop ensures the axial insertion below a certain torque threshold, as determined by the operator. This threshold also dictates the required level of the concrete softening, and consequently the level of noise emitted by the rotational reamer cutting (in a tradeoff with the drilling speed). Another feedback loop autonomously controls the adaptive impedance matching function, which does not require the operator involvement in normal conditions.

The three-stub tuner, incorporated with the waveguide-to-coax transition, and the adaptive tuning procedure are depicted in Fig. 7(a)–(c). The stepper motors drive the three stubs according to the tuning algorithm performed by the programmable controller. The power reflected from the load is sampled and analyzed throughout the drilling process. The push-pull manipulation of each stub is conducted until the reflected power is minimized to the permitted level. (The reflected power is normally kept below 5% of the transmitted power.) The adaptive impedance matching is autonomously activated in the automatic and manual operating modes. In a case of a convergence failure, a reset command reinitiates the matching process.

The remote hand-held operating box [Fig. 6(b)] maintains a serial communication with the main unit by another programmable controller (embedded in the operating box). It displays the drilling progress and the actual operating conditions, and enables commands such as mode selection (manual or automatic), power-level adjustment, and torque-limit setting for the rail-motor feedback.

The leading-rail basis has to be firmly attached to the drilled body, and covered by a metallic foil to avoid microwave leakage. Microwave leak detectors are incorporated in the MWD system in order to ensure the operator's safety. The common safety standard for microwave emission from domestic and industrial microwave installations (<1 mW/cm^2) [31] is satisfied in a proper MWD operation. The fixed positioning is also essential for the MWD stable alignment and proper operation in drilling deep holes (e.g., to reduce friction and avoid geometrical locking). An effective fixation is achieved by anchors (possibly inserted by the MWD itself).

The MWD makes no dust. However, the molten debris appearing as glasslike shavings inside and outside the hole must be evacuated in order to obtain a hollow deep hole. The two main modes of operation tested for the debris removal are the following.

A. Mode I: A Stepwise Operating Mode

In this manual mode, the microwave-drilling process is performed in successive steps. Each operating cycle includes a microwave irradiation period of ∼45 s, followed by a mechanical action for the removal of the accumulated debris. The inner surface of the hole is mechanically reamed, either manually or by the coaxial structure shown in Fig. 5(a) and (b), in order to enable the next deeper step. The debris removal is possibly assisted by pulsing bursts of pressurized air (∼6 bar) through the drilling tube for a 1-s period in order to blow out the debris from the hole. The inherent drawbacks of this operating mode are the excessive cooling of the hotspot by the blown-air bursts, and its whistling sound.

B. Mode II: Simultaneous Hollow-Reaming Mode

In this automatic mode, the microwave power is continuously irradiated while the entire coaxial structure, with the helical grooves on its perimeter [Fig. 5(a) and (b)], is slowly rotating in order to cut and remove the debris. A modest air pressure (∼0.5 bar) is constantly applied in order to assist the debris removal. The combined mechanism of the MWD and hollow reamer enables a sustainable, continuous operation of the drill in concrete.

IV. Experimental Results

Various field tests of the MWD prototype have demonstrated its capability of drilling 26-cm-deep holes in concrete.

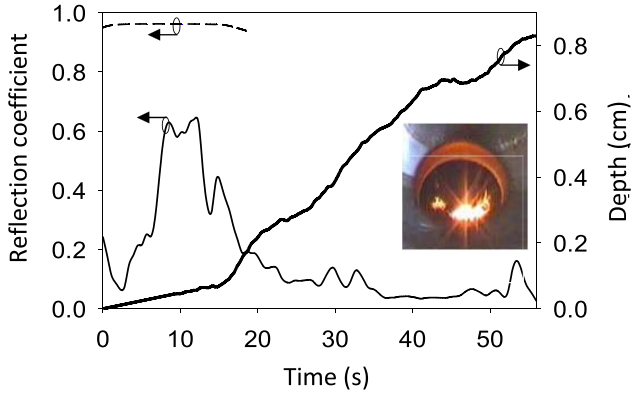

Fig. 8. Initial hotspot formation and the coaxial cylinder insertion into the molten concrete. The solid curves show the measured power-reflection coefficient and the drilling tube progress during the first minute period. The dashed curve represents the simulated reflection coefficient with no adaptive impedance matching. The inset shows the hotspot evolved on the surface, as observed through the view pipe depicted in Fig. 6(b) (a supplementary video clip is available[1]).

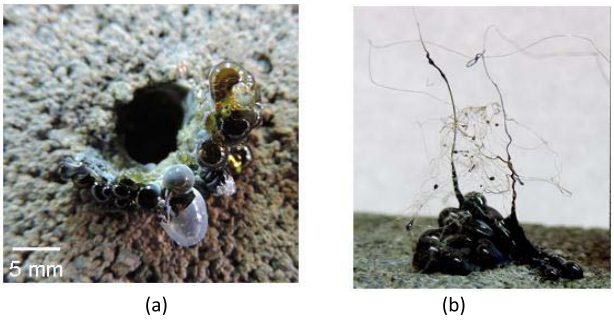

Fig. 9. Typical debris in glossy and hairy forms obtained by microwave drilling of concrete. (a) Molten debris vitrified in and out the drilled hole. (b) Glossy fibers produced by the air blown into the molten hotspot.

The average drilling speed measured in over one hundred field tests was ∼0.6 cm/min. The acoustic noise level detected was lower than 70 dBC (at a 1-m distance and a ∼40-dBC background noise level).

Laboratory experiments were conducted as well, using the same MWD prototype, in order to validate the field results. The experiments were conducted on standard pavement bricks (Wolfman Industries Inc., Model MP-3) of 8-cm thickness and 50-MPa concrete strength. The initial stage of a typical run in Mode II is presented in Fig. 8. An adaptive impedance matching sequence can be seen at the first ∼20-s period. Initially, the reflection coefficient tends to be relatively large, but later the autotuner reduces it to an acceptable level at steady state. The drilling speed is accordingly increased then.

Spontaneous byproducts of the microwave-drilling process in concrete are obtained in forms of glasslike shavings, as shown in Fig. 9(a) and (b). The molten concrete is resolidified and accumulated inside the hole and around it [Fig. 9(a)], whereas fibers made of the molten concrete ingredients [Fig. 9(b)] are formed by the pressurized air blow. These debris are removed by the hollow reamer during the MWD operation.

[1][Online]. Available: http://ieeexplore.ieee.org

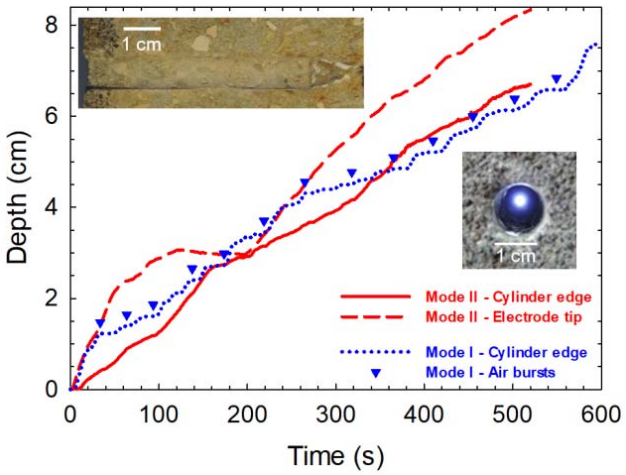

Fig. 10. Drilling depth progress versus time in Modes I and II. The arrows indicate the pressurized-air pulses in Mode I. The independent progresses of the electrode tip and the outer cylinder reamer edge are shown for Mode II. The insets show typical cross section cut and front view of the drilled holes.

Fig. 10 shows the drilling tube progress in typical MWD operations in modes I and II. The dotted-curve presents a stepwise drilling process in Mode I. In each operating cycle (of ∼45 s), the microwave irradiation is followed by a burst of pressurized air blow (∼6-bar pressure for a 1-s period) marked by a vertical arrow in the graph. Mode-I cycles also include mechanical removal of the debris, in order to shape the inner surface of the hole, and to enable a deeper insertion of the entire coaxial structure in the next cycle. A through-brick penetration (8-cm depth) was performed by 14 such cycles. The total microwave irradiation period (not including manual operations) was ∼10 min, hence the average net drilling speed is ∼0.65 cm/min in these Mode I experiments.

Fig. 10 also presents the fully automated Mode II of the MWD, as described above. The solid and dashed curves show the progress of the outer cylinder and the independent protrusion of the center electrode tip, respectively. The 12-mm diameter hole is drilled through the brick in <9 min. The reamer reached a depth of ∼6.7 cm just before the electrode tip punched through the outer surface of the brick (as shown in a side-cut and a front view images of the holes in the insets). An average drilling speed of ∼0.75 cm/min is demonstrated in this typical MWD run in Mode II. The similar net drilling speeds achieved in Modes I and II show that the full automation does not reduce the MWD net speed. Similar results were obtained in over sixty laboratory experiments.

The thermal-runaway and the hotspot propagation during the drilling progress are presented in Fig. 11(a) and (b), which show the final 150-s period (∼2-cm distance) of the drill-bit progress toward the exit surface of the brick. These results were obtained by a thermal camera (FLIR E40 camera) which captured the exit surface from $t = 387$ to 537 s, till the breakthrough moment. Fig. 11(a) shows the temperature profile evolution on the exit surface in this final 150-s period, as obtained from the thermal images (shown in the inset). The maximal temperature attained and the hotspot FWHM diameter are shown in Fig. 11(b) along with the electrode-tip progress in the brick. While the temperature on the

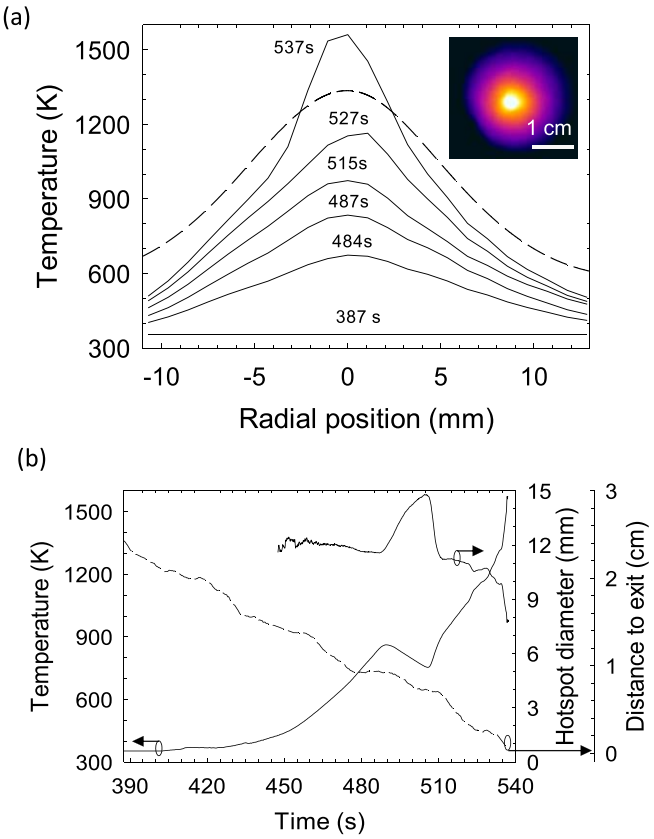

Fig. 11. Final 150-s period of microwave drilling through a concrete brick, before reaching its outer surface. (a) Temperature profile evolution at the exit surface, as the MWD bit is approaching it, obtained from FLIR thermal images as shown in the inset. The dashed curve shows the simulated hotspot profile [as in Fig. 3(c)] evolved on a surface located 5-mm away from the electrode tip, after a 100-s irradiation period. (b) Peak temperature measured on the exit surface, as the drill bit is approaching it, and the diameter (FWHM) of the hotspot observed on the outer surface.

outer surface rises, the diameter of the approaching hotspot decreases (due to its concentration by the thermal-runaway effect). At the breakthrough moment, the hotspot shrinks to a 7-mm width with a maximal temperature of 1550 K.

The MWD speed variations during the drilling operation (as in Figs. 10 and 11(b) for instance) can be attributed to the concrete inhomogeneity (due to aggregates, etc.). Another factor that significantly affects the MWD speed is the effectiveness of the debris evacuation. A significantly faster MWD drilling speed of >2 cm/min is typically achieved for short periods in the first penetration stage of the initial $\sim$1-cm depth (see Fig. 8). This higher drilling speed (>3 times faster than the average MWD speed) is attributed to the easier removal of the debris from the shallow holes, as compared to the deeper stages. These measurements also show the MWD potential speed capability, if not impeded by the debris removal, and they stress the need for a better removal mechanism incorporated in the MWD in order to expedite its overall drilling speed.

V. Discussion

The embedded adaptive impedance matching capability was found essential for tracking the rapid changes in the load impedance, from cold to hot conditions (or open-to-short circuit, respectively). The MWD's impedance matching is performed within 15–20 s, and hence the average TTM is of the same order. However, one may claim that the stepper-motor motion may not be sufficiently fast for the ultimate MWD applications. A heuristic TTM factor (as the drillability factor in [22]) may provide a rough estimate for the ideal (shortest possible) hotspot buildup time, derived from (2), as $\Delta t_{\min} \sim 2\rho c_p d_{hs}^3 \Delta T / P_{av}$ (assuming no thermal or radiation losses). This results in $\sim$5 s and $\sim$0.3 s ideal TTM estimates for 50-W and 850-W available microwave-power levels, respectively. In view of the typical $\sim$7-s tuning response time demonstrated in Fig. 7(c) ($\sim$30 steps of $\sim$0.2 s each), one may conclude that a faster tuning mechanism may lead to a significantly shorter TTM and hence to a much rapid MWD.

The numerical simulation results support the empirical measurements, though the theory does not take into account operational aspects, such as the tuning mechanism, moving and rotating parts, plasma, and air flow effects. However, the simulation demonstrates the MWD operating principle, and provides a reasonable estimate for its performance.

Among the various techniques considered for removing the MWD debris, the simultaneous hollow reaming (Mode II) seems to be more efficient, in terms of silence and speed, as compared to the other modes examined. This method allows drilling deep holes, continuously, with no human contact. The limitation of this technique stems from the narrower hotspot width ($\sim$10 mm) compared with the outer 12-mm diameter of the drill bit. The latter reams, therefore, into a less affected perimeter, which slows down the drilling operation.

VI. Conclusion

The portable MWD prototype presented in this paper has been proven to operate as a silent, remotely controlled drill for concrete. The noise level detected is satisfying for residential areas, even during night hours. The MWD vibration-free operation is attractive as well for occupied office areas, schools, and hospitals. In this respect, the MWD can be considered as an environmental friendly tool (compared to conventional mechanical drills). In these silent operating conditions, the MWD prototype is capable of drilling 26-cm-deep holes of 12-mm diameter, in an effective drilling speed of $\sim$0.6 cm/min, in concrete.

Additional improvements of the MWD technology are yet required, including a significant increase of the drilling speed (to at least 5 cm/min) and an ability to deal with iron rebars in reinforced concrete. The speed increase can be conceived, for example, by improving the overlap between the hotspot and the drill-bit area (so the cutting edge of the hollow reamer will encounter more softened concrete). A faster means for the adaptive impedance matching (instead of the stepper motors), and a more effective debris removal mechanism, may also expedite the drilling process. For rebar detection, further studies may include the incorporation of a short-range radar-like capability in the MWD system, in order to detect inhomogeneity, such as metallic barrier or air cavities, and hence to plan the drilling path accordingly. Rebar cutting could

be conceived, for example, by a plasma jet [32] ejected by the MWD.

The performance of the MWD prototype presented in this paper may not satisfy yet some practical concrete drilling needs. However, its silent, vibration-free MWD operation might be attractive for specific noise-sensitive applications. The experimental MWD results encourage more research and development, in order to effectively exploit this promising technology for silent drilling in concrete.

REFERENCES

[1] Z. Zhu, V. G. Dhokia, A. Nassehi, and S. T. Newman, "A review of hybrid manufacturing processes—State of the art and future perspectives," *Int. J. Comput. Integr. Manuf.*, vol. 26, pp. 596–615, Sep. 2013.

[2] V. Peržl, S. Hloch, H. Tozan, M. Yagimli, and P. Hreha, "Comparative analysis of abrasive waterjet (AWJ) technology with selected unconventional manufacturing processes," *Int. J. Phys. Sci.*, vol. 6, pp. 5587–5593, Sep. 2011.

[3] J. Kumar, "Ultrasonic machining—A comprehensive review," *Mach. Sci. Technol.*, vol. 17, pp. 325–379, Apr. 2013.

[4] W. Schulz, U. Eppelt, and R. Poprawe, "Review on laser drilling I. Fundamentals, modelling, and simulation," *J. Laser Appl.*, vol. 25, no. 1, 2013, Art. no. 012006.

[5] Y. Bar-Cohen and K. Zacny, Eds., *Drilling in Extreme Environments: Penetration and Sampling on Earth and Other Planets*. Weinheim, Germany: Wiley, 2009.

[6] Y. Bar-Cohen *et al.*, "High-temperature drilling mechanisms," in *High-Temperature Materials and Mechanics*, Y. Bar-Cohen, Ed. Boca Raton, FL, USA: CRC Press, 2014.

[7] A. C. Metaxas, *Foundations of Electroheat—A Unified Approach*, Chichester, U.K.: Wiley, 1996.

[8] S. Chandrasekaran, S. Ramanathan, and T. Basak, "Microwave material processing—A review," *AIChE J.*, vol. 58, pp. 330–363, Apr. 2012.

[9] G. Ong and A. Akbarnezhad, *Microwave-Assisted Concrete Technology: Production, Demolition and Recycling*, Boca Raton, FL, USA: CRC Press, 2015.

[10] N. Makul, P. Rattanadecho, and D. K. Agrawal, "Applications of microwave energy in cement and concrete—A review," *Renew. Sustain. Energy Rev.*, vol. 37, pp. 715–733, Apr. 2014.

[11] A. Buttress, A. Jones, and S. Kingman, "Microwave processing of cement and concrete materials—Towards an industrial reality?" *Cement Concrete Res.*, vol. 68, pp. 112–123, Sep. 2015.

[12] N. Makul, B. Chatveera, and P. Ratanadecho, "Use of microwave energy for accelerated curing of concrete: A review," *Songklanakarin J. Sci. Technol.*, vol. 31, pp. 1–13, Sep. 2009.

[13] R. V. Silva, J. de Brito, and R. K. Dhir, "Properties and composition of recycled aggregates from construction and demolition waste suitable for concrete production," *Constr. Build. Mater.*, vol. 65, pp. 201–217, Jun. 2014.

[14] A. Akbarnezhad, K. S. C. Kuang, and K. C. G. Ong, "Temperature sensing in microwave heating of concrete using fibre Bragg grating sensors," *Mag. Concrete Res.*, vol. 63, pp. 275–285, Aug. 2011.

[15] G. Roussy, A. Bennani, and J. Thiebaut, "Temperature runaway of microwave irradiated materials," *J. Appl. Phys.*, vol. 62, pp. 1167–1170, May 1987.

[16] C. A. Vriezinga, S. Sánchez-Pedreño, and J. Grasman, "Thermal runaway in microwave heating: A mathematical analysis," *Appl. Math. Model.*, vol. 26, pp. 1029–1038, Nov. 2002.

[17] E. Jerby, V. Dikhtyar, O. Aktushev, and U. Grosglick, "The microwave drill," *Science*, vol. 298, pp. 587–589, Sep. 2002.

[18] E. Jerby and V. Dikhtyar, "Drilling into hard non-conductive materials by localized microwave radiation," in *Proc. AMPERE-8 Int. Conf. Microw. RF Heating*. Bayreuth, Germany, Sep. 2001, pp. 687–694.

[19] E. Jerby and V. Dikhtyar, "Method and device for drilling, cutting, nailing and joining solid non-conductive materials using microwave radiation," U.S. Patent 6 114 676, Sep. 5, 2000.

[20] E. Jerby, O. Aktushev, and V. Dikhtyar, "Theoretical analysis of the microwave-drill near-field localized heating effect," *J. Appl. Phys.*, vol. 97, Sep. 2005, Art. no. 034909.

[21] Y. Eshet, R. R. Mann, A. Anaton, T. Yacoby, A. Gefen, and E. Jerby, "Microwave drilling of bones," *IEEE Trans. Biomed. Eng.*, vol. 53, no. 6, pp. 1174–1182, Jun. 2006.

[22] Y. Meir and E. Jerby, "Localized rapid heating by low-power solid-state microwave drill," *IEEE Trans. Microw. Theory Techn.*, vol. 60, no. 8, pp. 2665–2672, Aug. 2012.

[23] Y. Meir and E. Jerby, "The localized microwave-heating (LMH) paradigm—Theory, experiments, and applications," in *Proc. GCMEA*, Long Beach, CA, USA, Jul. 2012, pp. 131–145.

[24] E. Jerby, "Localized microwave-heating intensification—A 1-D model and potential applications," *Chem. Eng. Process. Intensification*, to be published. [Online]. Available: http://dx.doi.org/10.1016/j.cep.2017.02.008

[25] E. Jerby, Y. Shamir, R. Peleg, and Y. Aharoni, "A silent mechanically-assisted microwave-drill for concrete with integrated adaptive impedance matching," in *Proc. AMPERE Int. Conf. Microw. RF Heatin*, Nottingham, U.K., Sep. 2013, pp. 267–270.

[26] Y. Nerovny, O. Korin, and E. Jerby, "Performance tests of a silent microwave-drill for concrete," in *Proc. GCMEA-3*, Cartagena, Spain, Jul. 2016, pp. 162–165.

[27] J. M. Catalá-Civera, A. J. Canós, P. Plaza–González, J. D. Gutiérrez, B. García-Baños, and F. L. Peñaranda-Foix, "Dynamic measurement of dielectric properties of materials at high temperature during microwave heating in a dual mode cylindrical cavity," *IEEE Trans. Microw. Theory Techn.*, vol. 63, no. 9, pp. 2905–2914, Sep. 2015.

[28] S. Soldatov, M. Umminger, A. Heinzel, G. Link, B. Lepers, and J. Jelonnek, "Dielectric characterization of concrete at high temperatures," *Cement Concrete Compos.*, vol. 73, pp. 54–61, Sep. 2016.

[29] U. Schneider, "Concrete at high temperature—A general review," *Fire Safety J.*, vol. 13, pp. 55–68, Apr. 1988.

[30] V. Bilik and J. Bezek, "Automatic impedance matching under high power complex signal conditions," in *Proc. IMPI-48 Annu. Symp.*, New Orleans, LA, USA, Jun. 2014, pp. 6–9.

[31] *IEEE Standard for Safety Levels With Respect to Human Exposure to Radio Frequency Electromagnetic Fields 3 kHz to 300 GHz*, IEEE Standard C95.1, 2005.

[32] S. Popescu *et al.*, "Plasma column and nano-powder generation from solid titanium by localized microwaves in air," *J. Appl. Phys.*, vol. 118, p. 023302, Sep. 2015.

Eli Jerby received the Ph.D. degree in electrical engineering from Tel Aviv University, Tel Aviv, Israel, in 1989.

He completed his post-doctoral research at the Massachusetts Institute of Technology, Cambridge, MA, USA, as a Rothschild and Fulbright Post-Doctoral Fellow with the Research Laboratory of Electronics. He is currently a Professor with the Faculty of Engineering of Tel Aviv University, Tel Aviv, Israel. He studied novel schemes of microwave radiation sources (free-electron and cyclotron-resonance masers), and microwave-induced plasmas (plasmoids and fireballs). His recent studies deal with effects of localized microwave heating (LMH) and their applications (the microwave-drill invention, LMH-based additive manufacturing, thermite ignition, etc.).

Dr. Jerby served as the Editor of the *Journal of Microwave Power and Electromagnetic Energy* from 2006 to 2009 and is currently the Editor of the *AMPERE Newsletter*.

Yuri Nerovny was born in Donetsk, Ukraine, in 1992. He received the B.Sc. degree in electrical engineering from Tel Aviv University, Tel Aviv, Israel, in 2014, where he is currently pursuing the M.Sc. degree at the Department of Physical Electronics, under the supervision of Prof. Eli Jerby.

His current research interests include microwave localization, microwave-drill technology, localized microwave heating (LMH) effects, and additive solidification of metal powders by LMH.

Yehuda Meir was born in Bat-Yam, Israel, in 1983. He received the M.Sc. (*cum laude*) and Ph.D. degrees in electrical engineering from Tel Aviv University, Tel Aviv, Israel, in 2011 and 2016, respectively, under the supervision of Prof. Eli Jerby with the Department of Physical Electronics.

His current research interests include localized microwave heating (LMH), microwave drilling, thermite ignition, and fireballs and plasmoids, in both scientific and technological aspects.

Dr. Meir was the recipient of the Best Poster Award of the 13th AMPERE International Conference on Microwave and High Frequency Heating, Toulouse, France, in 2011, for his study on rapid heating by localized microwaves. He was the recipient of the Colton Scholarship in 2012.

Or Korin received the B.Sc. degree in electrical engineering from Tel Aviv University, Tel Aviv, Israel, in 2014, where he is currently pursuing the M.B.A. degree.

He is currently a System Engineer of wireless communications with the Israeli Defense Forces, as an officer with the rank of Captain.

Ron Peleg received the B.Sc. and M.Sc. degrees in electrical engineering from Tel Aviv University, Tel Aviv, Israel, in 2009 and 2016, respectively.

His current research interests include millimeter-wave RF integrated circuit, antennas, and RF system design.

Yariv Shamir was born in Kibbutz Ein Ge'di, Israel, in 1974. He received the B.Sc. degree in electrical engineering from Tel Aviv University, Tel Aviv, Israel.

He was an Engineer and Instructor with Prof. Jerby's laboratory at Tel Aviv University, from 2006 to 2009. In 2008, he joined the start-up company Scilense Microwave Ltd., Rishon LeZion, Israel, as a System Engineer. Since 2011, he has been with Agamit Ltd., Ramot Hashavim, Israel, where he is currently the Chief Executive Officer.